IEEE Access
Multidisciplinary ⋮ Rapid Review ⋮ Open Access Journal

Received 5 September 2022, accepted 14 September 2022, date of publication 22 September 2022, date of current version 17 October 2022.

Digital Object Identifier 10.1109/ACCESS.2022.3208954

RESEARCH ARTICLE

Reactively Loaded Dielectric-Based Antenna Arrays With Enhanced Bandwidth and Flat-Top Radiation Pattern Characteristics

RONIS MAXIMIDIS[1,2], DIEGO CARATELLI[1,3], (Senior Member, IEEE), GIOVANNI TOSO[4], (Senior Member, IEEE), AND A. BART SMOLDERS[1], (Senior Member, IEEE)

[1]Electromagnetics Group, Department of Electrical Engineering, Eindhoven University of Technology, 5600 MB Eindhoven, The Netherlands
[2]Wireless and Photonic Systems and Networks Research Group, Department of Informatics, Aristotle University of Thessaloniki, 54124 Thessaloniki, Greece
[3]Department of Research and Development, The Antenna Company, 5656 AE Eindhoven, The Netherlands
[4]Radio Frequency Payloads & Technology Division, Antenna and Sub-Millimeter Waves Section, European Space Agency, ESA ESTEC, 2200 AG Noordwijk, The Netherlands

Corresponding author: Ronis Maximidis (r.t.maximidis@tue.nl)

This work was supported in part by the Network/Partnering Initiative between the European Space Agency, in part by The Antenna Company, and in part by the Eindhoven University of Technology under Contract 4000114668/15/NL/MH.

ABSTRACT This paper presents an antenna array organized in sub-arrays and composed of densely spaced dielectric-based radiating elements. To reduce the number of active components required in the array beamforming network, each sub-array consists of a single active element, directly fed, and several passive reactively loaded elements. State-of-the-art implementations of such arrays are typically based on rectangular air-filled waveguide radiators which provide a limited bandwidth and support a single linear polarization only. By utilizing the dielectric-based radiators presented in this work, a significant increase in the operating bandwidth of the array can be achieved. In this case, the aforementioned reactive loading is implemented through short-circuited dielectric-filled waveguides. By optimizing the position of the short circuits, the radiation pattern of the sub-array can be controlled and synthesized according to a given mask. To create larger design flexibility, one can design the sub-array in the presence of the adjacent sub-arrays, achieving in this way their effective overlapping. By employing the considered design technique, a sub-array featuring flat-top radiation pattern characteristics in combination with low side-lobe levels and high gain was developed, manufactured, and thoroughly analyzed. An additional benefit of such a design choice is the possibility of supporting two orthogonal polarizations.

INDEX TERMS Dielectric, antennas, waveguides, overlapping, flat-top, reactive, loads, passive, sub-array, arrays.

I. INTRODUCTION

Modern satellite and terrestrial communication networks require high flexibility and control in terms of radiation pattern reconfigurability. At the antenna level, this can be achieved by adopting active antenna array architectures with electronically controllable beam-steering and multi-beam capabilities [1], [2]. The radiation characteristics of an antenna array depend on the position and excitation of the relevant radiating elements, as well as on the type of adopted antenna technology. Although active antenna arrays provide maximum performance flexibility, the relevant costs of implementation and the required power levels are prohibitive for most practical applications, even when arrays of moderate size are considered [3]. In order to deal with these limitations, various antenna array design architectures were proposed [4], [5], [6], [7], [8], [9], [10], [11], [12], [13].

In the case where the required field of view (FoV) is limited, a cost-effective antenna array solution can be realized by combining the radiating elements in sub-arrays and using

The associate editor coordinating the review of this manuscript and approving it for publication was Lu Guo.

one transmit/receive channel per sub-array. The disadvantage of such a configuration is the significant separation between the phase center of the various sub-arrays that is typically larger than half-wavelength at the frequency of operation, this leading to the appearance of grating lobes unless these are properly filtered by a flat-top radiation pattern at the level of individual sub-array. Many radiating structures have been proposed in the scientific literature to achieve flat-top radiation pattern characteristics [14], [15], [16], [17], [18], [19]; however, due to their specific geometries [15], [19] and large dimensions in combination with broad beamwidth [14], [16], [17], [18], there is no easy way to adopt those as radiating elements in an array structure, which is meant to deliver high gain and grating lobe free radiation even though in a limited scanning range.

To achieve effective control of the sub-array radiation characteristics while maintaining a large aperture of the radiating elements, the same radiating elements can be re-used in the adjacent sub-arrays achieving, in this way, a sub-array overlapping. A comprehensive overview of antenna arrays with sophisticated feeding structures enabling overlapping use can be found in [4]. Moreover, a recent example of a feeding network with overlapping functionality is presented in [7]. However, such a feeding network is very complex even for arrays with a small number of radiating elements; hence, this implementation concept has found limited application. The complexity of the feeding network can be simplified significantly by using array topologies consisting of both directly fed radiating elements and parasitic passive elements terminated on suitable loads. In such a configuration, the passive elements are fed via a free-space coupling mechanism. Examples of such a configuration can be found in [5] and [6] for dipole arrays whose beam-scanning characteristics are controlled by adjusting loads of suitable parasitic elements. In [10], [11], and [12], the radiated beam of waveguide antenna arrays is shaped by reactive loading of parasitic waveguiding elements. In a more recent study [13], complex magneto-electric dipoles have been used to enhance the antenna's directivity.

In [20], we designed and realized an array of sub-arrays composed of open-ended waveguide antenna elements. In the considered design, the reactive loads were implemented by parasitic waveguides terminated on short circuits and by properly selecting the relevant length. In this way, we were able to shape the radiation pattern of the individual sub-array and control the scattering parameters at the corresponding ports. The analysis of the radiation properties of a simplified version of such a structure, composed of identical passive metallic waveguide elements, is presented in [21], where multiple electromagnetic radiation regimes involving volume, surface, and leaky waves were identified for the considered class of antennas. The increased complexity of the radiating structure proposed in this study prevents the application of the analysis methodology used in [21]. On the other hand in [20], we have developed a coherent design methodology for reactively loaded overlapping sub-arrays design which is not constrained by the shape and type of the waveguides. The sub-array overlapping was also achieved by taking advantage of the mutual coupling process which occurs between adjacent waveguiding elements. The array structure detailed in [20], however, suffers from a limited operational bandwidth that reduces its practical use. To overcome the aforementioned limitation, we propose here to use reactively loaded dielectric-based radiating elements. As was shown in [22], an additional benefit of such a design choice is the possibility of supporting two orthogonal polarizations.

This paper is organized as follows. Section II presents the framework of the semi-analytical design technique implemented for the design of the reactively loaded sub-array. Section III starts with the analysis of the performance of the radiating element and justifies its choice. Next, a linear array of 3-sub-arrays is designed and analyzed. Section III concludes with a theoretical analysis of the performance of a large array based on the previously designed sub-array. In Section IV, the 3-sub-array prototype is presented, and its performance is compared with the theoretical study of Section III. Concluding remarks are summarized in Section V.

II. METHODOLOGY

A schematic of an antenna array of randomly distributed N_a directly-fed active elements and N_p reactively-loading passive elements is shown in Fig. 1. The optimization of the terminations of the various passive elements using a full-wave electromagnetic (EM) solver is extremely time-consuming. Therefore, to reduce the development time, we exploit the semi-analytical design methodology developed by the authors in [20] that is summarized hereafter.

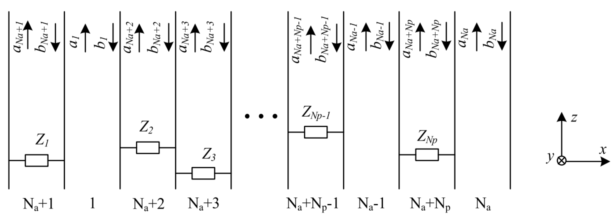

FIGURE 1. Schematic view of a reactively loaded antenna array [20].

According to [20], the frequency-domain distribution of the total electric field $\vec{E}(\theta, \varphi)$ radiated by the array structure of Fig. 1 can be written as:

$$\vec{E}(\theta, \varphi) = \begin{bmatrix} \mathbf{a}_a^T & \mathbf{a}_a^T \end{bmatrix} \cdot \begin{bmatrix} \vec{\mathbf{E}}_a(\theta, \varphi) \\ \underline{\mathbf{S}}_c \cdot \left(\left[\left(\underline{\mathbf{\Gamma}}_p \cdot e^{-2\underline{\gamma}_p \cdot \underline{\mathbf{h}}_p} \right)^{-1} - \underline{\mathbf{S}}_p \right]^{-1} \right)^T \cdot \vec{\mathbf{E}}_p(\theta, \varphi) \end{bmatrix}, \tag{1}$$

with the superscript ^{T} denoting the matrix transposition and the subscripts a and p referring to the active and passive elements, respectively. Besides, θ and φ are the conventional spherical angles.

In (1), the vector $\mathbf{a}_a$ contains the excitation coefficients of the active, directly fed, radiators, whereas the vectors $\vec{\mathbf{E}}_a(\theta, \varphi)$ and $\vec{\mathbf{E}}_p(\theta, \varphi)$ are the electric fields radiated by the active and passive elements, respectively. Moreover, the matrices $\underline{\mathbf{S}}_p$ and $\underline{\mathbf{S}}_c$ denote the blocks of the complete array scattering matrix $\underline{\mathbf{S}}$ that describe, respectively, the interaction between passive waveguides and the coupling process between passive and active waveguides. Lastly, $\underline{\mathbf{\Gamma}}_p$, $\underline{\boldsymbol{\gamma}}_p$, and $\underline{\mathbf{h}}_p$ are diagonal matrices containing the reflection coefficients of the loads, the complex propagation coefficients, and lengths of the passive waveguides, respectively. In addition, the scattering matrix of the directly fed elements can be expressed as:

$$\underline{\mathbf{S}}'_a = \underline{\mathbf{S}}_a + \underline{\mathbf{S}}_c \cdot \left[(\underline{\mathbf{\Gamma}}_p \cdot e^{-2\underline{\boldsymbol{\gamma}}_p \cdot \underline{\mathbf{h}}_p})^{-1} - \underline{\mathbf{S}}_p \right]^{-1} \cdot \underline{\mathbf{S}}_c^T \qquad (2)$$

Here, $\underline{\mathbf{S}}_a$ is the block, in the complete array scattering matrix $\underline{\mathbf{S}}$, that describes the interaction between directly fed radiating elements.

By exploiting (1) and (2), the design of reactively loaded sub-arrays can be accomplished following the procedure hereafter:

1. Set the array topology and determine the minimum number N_S of sub-arrays needed to approximate an infinitely large array environment for the central sub-array element and fix the number of elements per sub-array N_E.
2. Determine the scattering matrix and the electric fields radiated by the $N_S \times N_E$ elements forming the array structure.
3. Choose a suitable optimization algorithm and set the proper optimization goals selecting from the set of available optimization parameters $[\underline{\mathbf{\Gamma}}_p, \underline{\boldsymbol{\gamma}}_p, \underline{\mathbf{h}}_p]$.
4. Use the central sub-array pattern as the embedded element pattern for the design of arrays of any size.

Utilizing the proposed design procedure, a reactively loaded array with a shaped radiation pattern and constrained scattering matrix characteristics can be developed and optimized. The proposed design procedure has been implemented in Matlab [23].

III. DESIGN

A. RADIATING ELEMENT

The choice of the radiating element plays a significant role during the antenna array design stage. First of all, in order to be able to shape the sub-array radiation pattern, the separation between array elements has to be smaller than $\lambda_0/2$, with λ_0 being the free-space wavelength. In [20] and [24], we used, as radiating elements, air-filled rectangular waveguides operating on their fundamental TE_{01} mode. This allowed us to keep one of the waveguide dimensions small to densely place the radiating elements and achieve efficient control of the sub-array radiation characteristics. Although we were able to design sub-arrays with nicely shaped radiation patterns and reduced active reflection coefficients at the selected working frequency, the radiation pattern stability over the frequency was rather limited. To overcome this limitation, in this study we propose to use dielectric radiators, terminated by dielectric-filled waveguides. The height of the dielectric radiator is optimized in such a way to achieve maximal radiation efficiency. For comparison reasons, the air-filled rectangular waveguide antenna array structure is shown in Fig. 2a, while in Fig. 2b an array of waveguides filled with extended dielectric rods is presented. In addition, in Fig. 2, the azimuth φ and elevation θ angles are defined. The rounding radius of the corners of the air-filled waveguide cross-sections is adjusted to achieve the same cut-off frequency as obtained with the dielectric-filled waveguides. In both configurations, the elements are excited by the TE_{01} waveguide mode. Table 1 presents the coupling levels between the central radiator, labeled as "1", and the adjacent elements on one side of each sub-array presented in Fig. 2. We can readily notice that the coupling levels achievable with the dielectric-based design are typically much larger than those obtained with the air-filled counterpart structure. Furthermore, the dielectric-based radiators are characterized by a reduced input reflection coefficient which translates into a smaller quality factor of the short-circuited "resonators" used as loading elements.

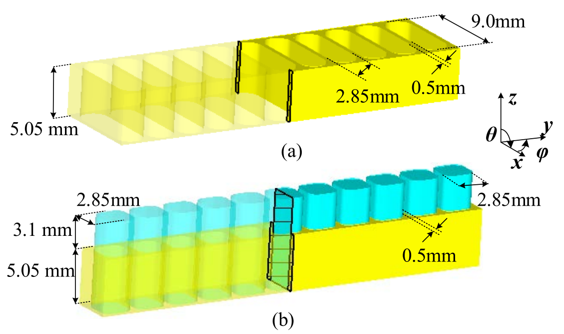

FIGURE 2. Three-dimensional view of the 11 × 1 antenna array of a) air-filled waveguides b) dielectric-filled waveguides with extended dielectric rods.

TABLE 1. Coupling coefficients between the central element and the 5 elements of one side of an 11 × 1 antenna array, f_0 = 20.0 GHz.

	S_{11} [dB]	S_{21} [dB]	S_{31} [dB]	S_{41} [dB]	S_{51} [dB]	S_{61} [dB]
Air	-7.11	-8.33	-15.45	-19.62	-22.75	-24.34
Diel.	-15.95	-14.19	-9.92	-11.28	-14.28	-18.74

B. SUB-ARRAY DESIGN

In the present work, the sub-array design procedure detailed in [20] was utilized. Such a procedure starts with the choice of the number N_S of integrated sub-arrays. To enable the overlapping between adjacent sub-arrays, we need to use $N_S \geq 3$. The simplest sub-array configuration which can be adopted is the one where an individual central directly-fed element is integrated with multiple passive elements symmetrically placed on both sides. In this study, we target an FoV of ±8.5° around the broadside in combination with an operational bandwidth BW = 500 MHz (19.7-20.2 GHz) at a 10-dB return-loss level. To ensure that the grating lobes are outside the FoV for all the scan angles, the sub-array spacing has to be $3.42\lambda_0$ or smaller wherein the roll-off of the relevant radiation pattern is properly accounted for [25]. Using the dimensions of the dielectric-based elements presented in the previous section while aiming for maximal sub-array separation of about $2.5\lambda_h$, where λ_h is the wavelength at the highest frequency of operation, we end up with a sub-array consisting of 11 elements and having a length $L = 2.48\lambda_h$. The selected separation places the first grating lobe at ±23.8° when the array is radiating along the broadside direction and at −15.3° degrees for the maximum scan angle $\theta_e = 8.5°$ [25].

The scattering matrix $\underline{\mathbf{S}}$ of the 3 × 11 elements array and the embedded radiated electromagnetic field distributions required for the application of the design algorithm were evaluated using a Finite Element Method (FEM) solver implemented in the commercial software CST Microwave Studio [26]. The numerical results collected in this way were then imported into a dedicated optimization tool, which relies on the numerical algorithm described in [20]. The lengths of the passive waveguide elements, $\underline{\mathbf{h}}_p$, were chosen as the design parameters in the sub-array optimization procedure and the following objective function was built:

$$\Psi_O\left(f,\underline{\mathbf{h}}_p\right)=\left[1-\left|S'_{11,a}\left(f,\underline{\mathbf{h}}_p\right)\right|\right]\cdot\left\{\min_{\theta\in[\theta_{SL},90°]}\frac{D(f,\underline{\mathbf{h}}_p,\theta_e)}{D(f,\underline{\mathbf{h}}_p,\theta)}\right.$$
$$\left.-\left|\int_0^{\theta_e}\left[D(f,\underline{\mathbf{h}}_p,\theta)-D(f,\underline{\mathbf{h}}_p,\theta_0)\right]d\theta\right|\right\}, \quad (3)$$

where D denotes the array directivity function and $S'_{11,a}$ is the input reflection coefficient of the active element of the central sub-array when the adjacent sub-arrays are terminated with matched loads. In (3), the two terms in brackets control the optimization of the array radiation pattern in terms of sidelobe level (SLL) for $\theta \in [\theta_{SL}, 90°]$ with $\theta_{SL} = 20°$ and in terms of flatness within the FoV for $\theta \in [0°, \theta_e]$. Since the considered array is symmetric, we can confine the analysis to the angular range $\theta \in [0, 90°]$

Upon focusing on the three (lower, middle, upper) frequencies $f_L = 19.7$ GHz, $f_0 = 20.0$ GHz, and $f_H = 20.2$ GHz, the design procedure is turned into the solution of the following minimization problem:

$$\underset{0\leq\underline{\mathbf{h}}_p\leq 0.5\lambda_g}{\arg\min}\left[-\Psi_O\left(f_L,\underline{\mathbf{h}}_p\right)-\Psi_O\left(f_0,\underline{\mathbf{h}}_p\right)-\Psi_O\left(f_H,\underline{\mathbf{h}}_p\right)\right], \quad (4)$$

where $\lambda_g = 10.1$mm is the guided wavelength corresponding to the TE_{01} mode of the dielectric-filled waveguide at the working frequency, $f_0 = 20$ GHz. Thanks to the symmetry of the sub-array structure, the number of design parameters is equal to half the number of passive waveguides.

The structure obtained by means of the presented design procedure is shown in Fig. 3, and the relevant optimized waveguide lengths are listed in Table 2, where the numbering starts from the element immediately adjacent to the central waveguide.

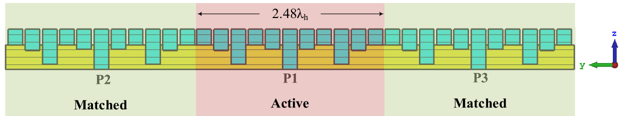

FIGURE 3. Schematic of the 3 sub-arrays array. Each sub-array consists of 11 radiating elements, one directly fed or terminated on a matched load and 10 reactively loaded in a symmetric placement around the central element.

TABLE 2. Waveguide lengths of the structure in Fig. 3.

	h_0	h_1	h_2	h_3	h_4	h_5
[mm]	5.05	0.85	0.03	3.81	1.09	0.00
[λ_g]@20GHz	0.5	0.084	0.003	0.377	01.08	0.000

To assess the overlapping effect, the central sub-array was directly fed while the feeding waveguides of the adjacent sub-arrays were terminated to their characteristic impedances, as it is shown in Fig. 3, and the electric field distribution of the central sub-array was analyzed at different frequencies (see Fig. 4). Fig. 4 clearly shows a strong field coupling process occurring across neighboring sub-arrays, especially at the highest end of the operational band.

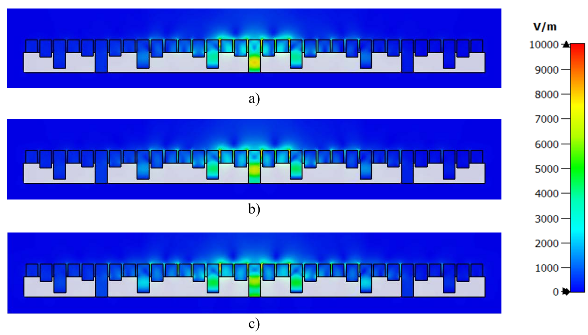

FIGURE 4. Electric field distribution along the cross-section of the 3-sub-array structure when the central sub-array element is excited at (a) $f_L = 19.7$ GHz, (b) $f_0 = 20.0$ GHz, and (c) $f_H = 20.2$ GHz.

Fig. 5 shows the E-plane directivity function at the three frequencies of interest, while Fig. 6 shows the cross-polarization discrimination (XPD) defined as co-polarization to cross-polarization ratio along the E-plane for the sub-array integrated as the central element in a 3-sub-array configuration at $f_L = 19.7$ GHz, $f_0 = 20.0$ GHz, and $f_H = 20.2$ GHz. The XPD characteristics displayed in Fig. 6 are evaluated in the ideal case of the central sub-array fed by

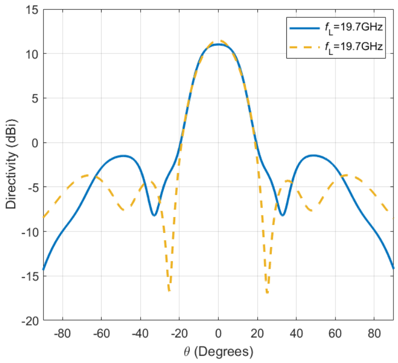

(a)

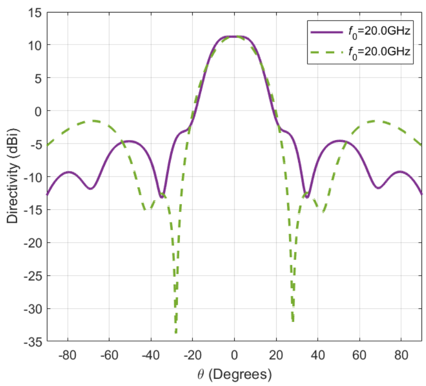

(b)

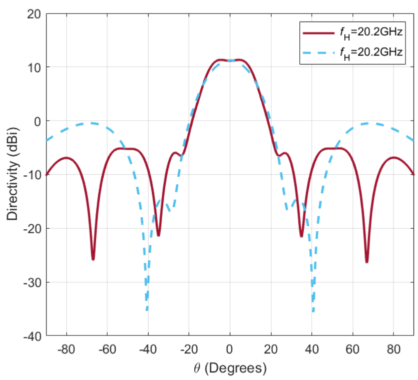

(c)

FIGURE 5. E-plane directivity function of the sub-array in standalone configuration (dashed line) and integrated as the central element in a 3-sub-array configuration at (a) $f_L = 19.7$ GHz, (b) $f_0 = 20.0$ GHz, and (c) $f_H = 20.2$ GHz.

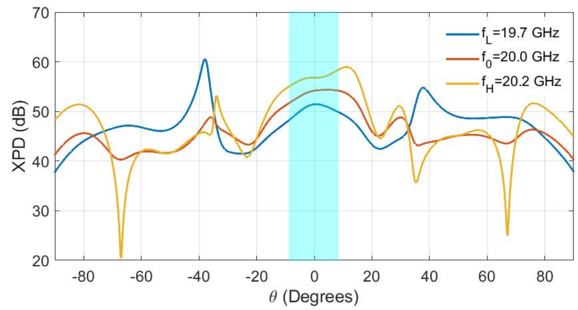

FIGURE 6. XPD, along the E-plane, of the sub-array integrated as the central element in a 3-sub-array configuration at $f_L = 19.7$ GHz, $f_0 = 20.0$ GHz, and $f_H = 20.2$ GHz.

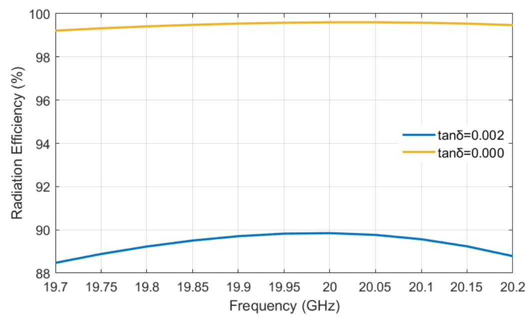

FIGURE 7. Radiation efficiency of the sub-array integrated as the central element in a 3-sub-array configuration.

a pure TE_{01} mode, without any feeding and holding structure included. One can notice that the designed antenna features a very low cross-polarization component with the XPD level being larger than 49 dB across the entire FoV.

The efficiency of the considered radiating structure is shown in Fig. 7. As it appears from Fig. 7, the designed sub-array features high radiation efficiency with a nearly flat distribution having a maximal fluctuation level of about 1.3%. For completeness, the sub-array performance has been evaluated, also, in the case of a lossless dielectric. By visual inspection of Fig. 7, it is clear that the dielectric losses cause a degradation of the radiation efficiency of up to about 10%.

C. SUB-ARRAY PERFORMANCE

In Fig. 8, the input reflection coefficient of the central sub-array and the coupling coefficients relevant to the optimized 3-sub-array configuration are shown. Thanks to the symmetry of the structure, the corresponding behavior can be characterized by means of a reduced number of scattering parameters. Fig. 8 shows that the coupling level between sub-arrays is lower than −20dB nearly across the entire band. On the other hand, the magnitude of S_{11} is somehow larger than −10dB at low frequencies; however, it can be improved by integrating a suitable impedance matching circuit.

A feeding structure consisting of a pin integrated into a short-circuited waveguide parallel to the electric field of the TE_{01} mode was adopted for the feeding of individual active elements. The position of the pin along the waveguide and its length were optimized in such a way as to enhance the impedance matching across the entire frequency band. The schematics of the feeding section is shown in Fig. 9, while the relevant dimensions are listed in Table 3.

Two additional 0.5-mm holes were realized in the waveguide structure so to make use of suitable tuning screws, in order to be able to adjust the input impedance characteristics after manufacturing. The distance between the waveguide

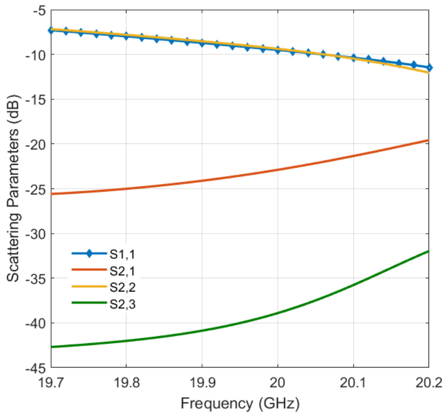

FIGURE 8. Reflection coefficient and coupling level between sub-arrays of the 3 × 11 antenna array structure of Fig. 3.

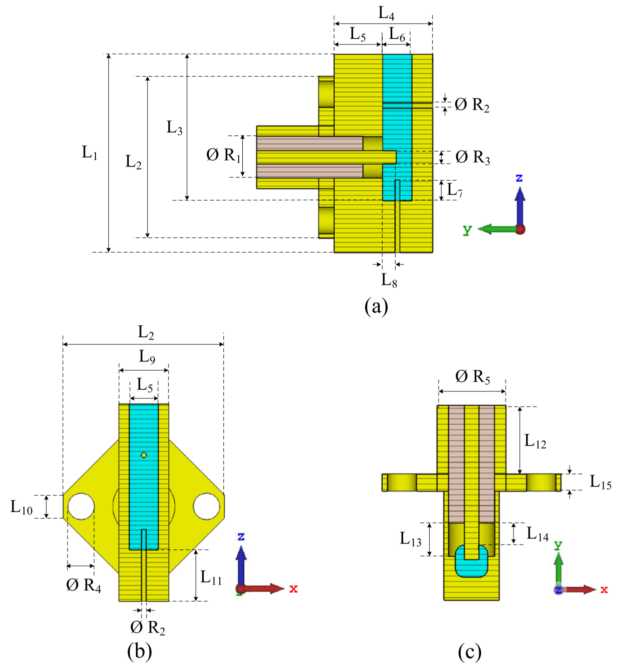

FIGURE 9. Different cut-sections of the array feeding structure: (a) yz-cut, (b) xz-cut, and (c) xy cut.

aperture and the center of the screw hole and the connector is 4.97 mm and 9.97 mm, respectively.

In Fig. 10 are presented the E-plane distributions of the directivity function obtained for 3-, 5-, and 7-sub-array configurations. One can readily observe that the integration of the first two sub-arrays next to the central one has a small but noticeable impact on the radiation characteristics. On the other hand, the integration of the additional sub-arrays produces rather marginal effects. In the light of this, the directivity function of the central sub-array in the 7-sub-array configuration was selected as the embedded directivity function in the synthesis procedure of arrays of arbitrary size; the relevant main characteristics are reported in Table 4 for completeness.

TABLE 3. Dimensions of the feeding structure.

L_1	19.20 mm	L_{11}	5.00 mm
L_2	15.70 mm	L_{12}	6.00 mm
L_3	14.20 mm	L_{13}	2.90 mm
L_4	9.55 mm	L_{14}	1.90 mm
L_5	4.70 mm	L_{15}	1.50 mm
L_6	2.85 mm	R_1	4.06 mm
L_7	2.00 mm	R_2	0.50 mm
L_8	1.30 mm	R_3	1.28 mm
L_9	4.85 mm	R_4	2.60 mm
L_{10}	2.26 mm	R_5	6.06 mm

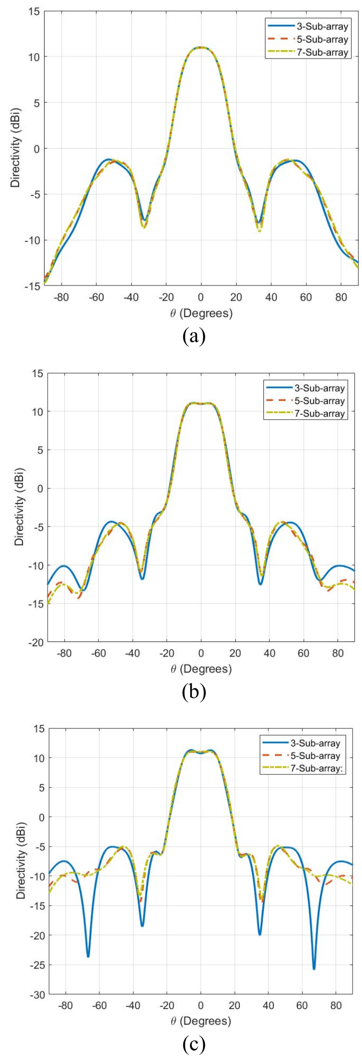

FIGURE 10. E-plane directivity function of the central sub-array integrated in different array configurations at (a) $f_L = 19.7$ GHz, (b) $f_0 = 20.0$ GHz, and (c) $f_H = 20.2$ GHz.

In Fig. 11, the input reflection coefficient of the active element of the central sub-array and the relevant coupling coefficients to the adjacent sub-arrays are shown and

TABLE 4. Radiation characteristics of the central sub-array of the array consisting of 7 sub-arrays across the frequency band of interest.

f [GHz]	$D_{iniform}$ [dBi]	$D(\theta=0^o)$ [dBi]	$D(\theta=8.5^o)$ [dBi]	$D(\theta=15.3^o)$ [dBi]	SLL [dB]
19.7	11.63	10.99	9.72	4.24	-12.21
20.0	11.74	11.01	10.59	3.68	-15.43
20.2	11.80	10.96	10.53	4.89	-15.84

compared when considering arrays of 3, 5, and 7 identical sub-arrays. As it can be noticed, a good impedance matching has been achieved across the entire frequency range of operation, with a slight degradation at the lower sub-band. Fig. 11 shows, also, that the input reflection coefficient remains practically unaffected when additional sub-arrays are integrated thanks to the low coupling level between sub-arrays. On the other hand, as the number of sub-arrays increases from 3 to 5, a reduced impact on the S_{21} coefficient is observed. A further increase in the number of sub-arrays, however, does not cause any noticeable change in the coupling level between the central sub-array and the immediately adjacent one. Here it is worth mentioning that in the 7-sub-array configuration the coupling level to other sub-arrays which are further apart from each other is well below −35 dB. This clearly indicates that the surface wave component excited by the central active waveguide element does not propagate farther than the first adjacent sub-array.

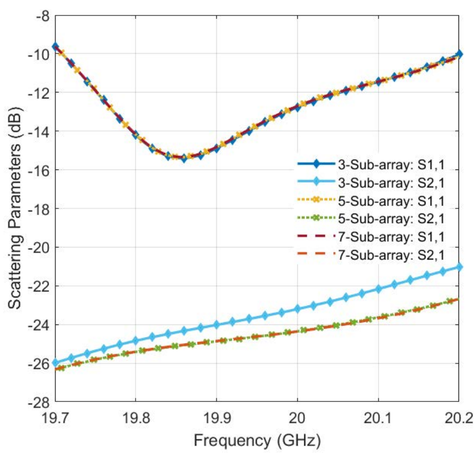

FIGURE 11. Input reflection coefficient and coupling level in different array configurations. The port numbering is according to Fig. 3.

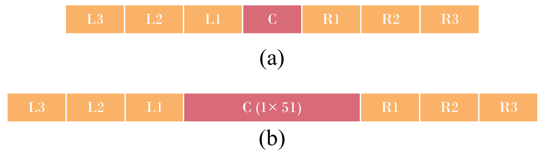

FIGURE 12. Schematic representation of (a) 7 sub-array and (b) 57 sub-array array structures inclusive of the relevant edge elements.

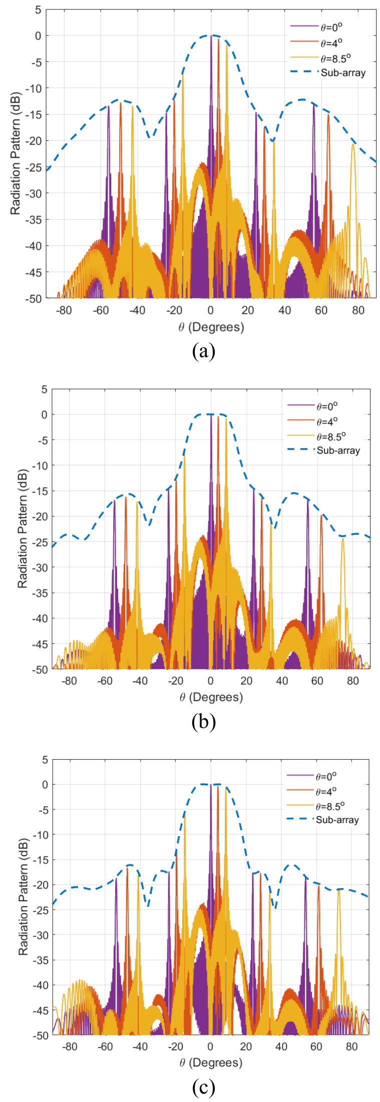

FIGURE 13. E-plane radiation pattern of the array of 57 overlapping sub-arrays of dielectric-loaded radiating structures at (a) $f_L = 19.7$ GHz, (b) $f_0 = 20.0$ GHz, (c) $f_H = 20.2$ GHz. The embedded radiation pattern of the central sub-array at the considered frequencies is included as well.

D. CASE STUDY: ARRAY OF 57 SUB-ARRAYS

The use of the design sub-array in a large array configuration is presented in this section. The case study concerns the design of a linear array featuring a half-power beamwidth of 0.5° around the broadside direction in the relevant E-plane, which requires an integration of $N_S = 57$ sub-arrays. In order to properly account for the edge effects during the array design stage, the technique implemented in [24] was adopted, and to this end, the considered 57-sub-array structure was segmented as illustrated in Fig. 12.

In Fig. 13, the radiation pattern of the designed array is shown for three relevant scan angles at the aforementioned frequencies $f_L = 19.7$ GHz, $f_0 = 20.0$ GHz, and

TABLE 5. Radiation characteristics of the 57-sub-array array.

Frequency f [GHz]	Scan Angle θ [°]	Directivity [dBi]	1st Grating Lobe [dB]	2nd Grating Lobe [dB]
19.7	0.0	28.56	-14.71	-13.36
	4.0	27.89	-11.56	-12.11
	8.5	26.88	-5.67	-11.77
20.0	0.0	28.58	-14.61	-16.91
	4.0	28.10	-12.45	-15.70
	8.5	27.74	-6.49	-16.42
20.2	0.0	28.52	-17.42	-18.62
	4.0	28.13	-12.92	-16.25
	8.5	27.66	-4.85	-17.22

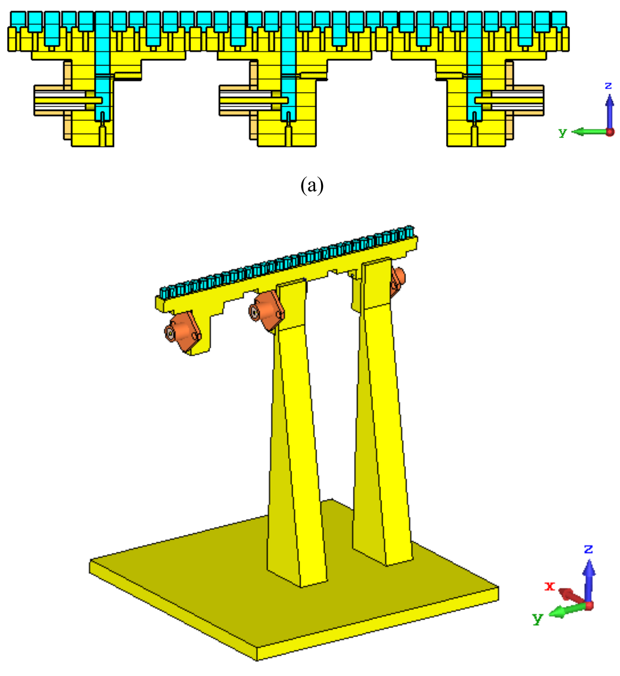

FIGURE 14. Model of the manufactured array demonstrator: (a) 3-sub-array cross-section, (b) isometric view of the array inclusive of the mounting structure.

TABLE 6. Actual dimensions of the connectors in the realized prototype.

	pin [mm]	cover [mm]
Original, all	6.0	2.8
Port #1	5.91	3.2
Port #2	6.08	3.4
Port #3	5.92	3.23

$f_H = 20.2$ GHz for three different scan angles. It is apparent that the grating lobes are filtered effectively in the case of broadside illumination for all three frequencies. However, as the scan angle moves away from the $\theta = 0°$ direction, the first grating lobe moves closer to the boresight, this causing a

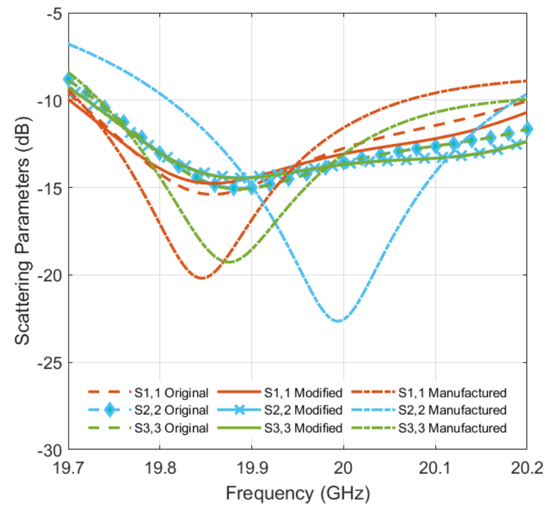

FIGURE 15. Reflection coefficient of the original array structure (solid line), of the array demonstrator including the mounting structure shown (dashed line), and of the array model with the actual dimensions of the connectors integrated into the real-life prototype (dash-dotted line).

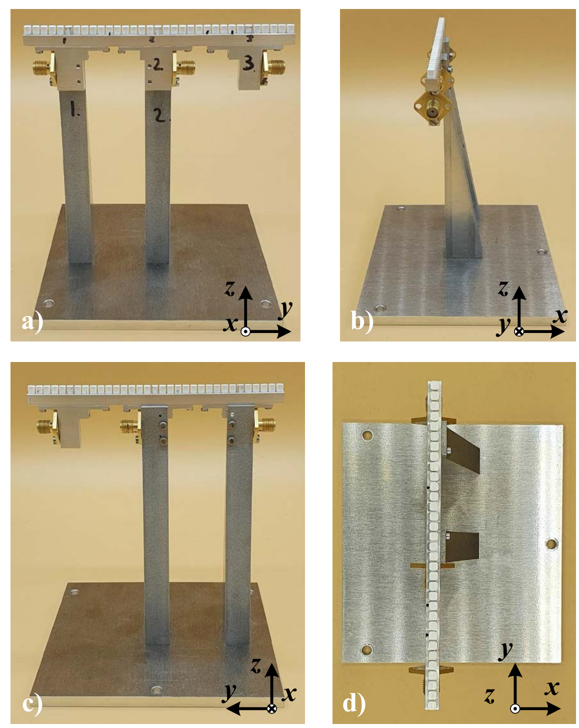

FIGURE 16. Prototype of the array of three sub-arrays of dielectric-based reactively loaded waveguide antennas inclusive of mounting structure: a) front view, b) right view, c) back view, d) top view.

decrease in the relevant rejection level in the measure of the sub-array element pattern.

Table 5 summarizes the array characteristics at the considered frequencies. From Table 5, we can conclude that the boresight directivity is nearly constant over the entire frequency range of interest while having some decrease when scanning. In addition, the rejection level of the first grating

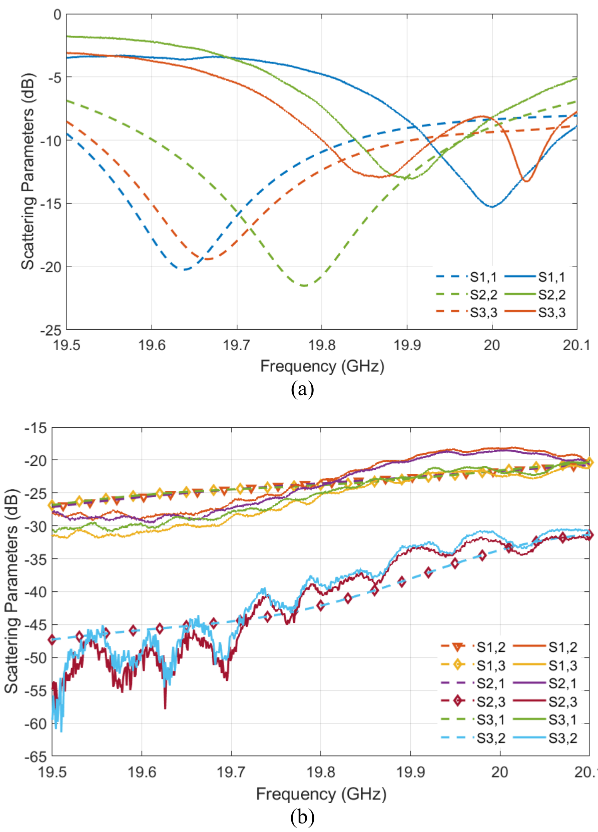

FIGURE 17. Measured (solid line) and simulated (dashed line) (a) reflection coefficients and (b) coupling coefficients, of 3 sub-arrays antenna array. The simulation model is based on dielectric parts with relative permittivity $\varepsilon_r = 10.23$.

lobe degrades while scanning to the edge of the FoV. In practical applications, the scan range can be limited so to ensure the required rejection level over the entire frequency band of operation.

IV. PROTOTYPE

To validate the design concept proposed in this research study, an array of three sub-arrays has been manufactured and thoroughly studied. The relevant model, inclusive of the mounting structure, is shown in Fig. 14.

The mounting structure consists of two metal pillars having a length of 108.95 mm and a tapered profile with thickness varying from 20 mm down to 2 mm. The feeding elements of the array are directly attached to the supporting pillars which, in turn, are fixed on a metal plate with dimensions of 97.85 mm × 106 mm × 5 mm. In order to increase reliability, holes with a radius of 1 mm were realized in the center of each short circuit wall, so to let air escape during the press-filling process implemented for the fixation of the dielectric rods inside the passive waveguides.

During the manufacturing process, some deviations were noticed in the dimensions of the pins integrated in the connectors. In view of this, the array model was modified

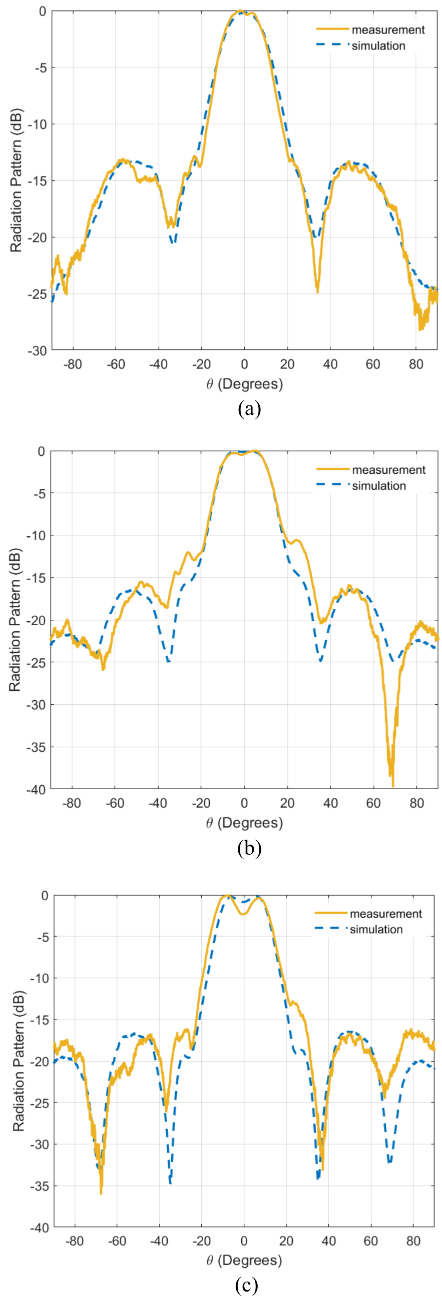

FIGURE 18. Comparison between the measured and simulated E-plane radiation pattern at (a) $f_L = 19.5$GHz, (b) $f_0 = 19.8$GHz, and (c) $f_H = 20.0$GHz with the relative permittivity of the dielectric filling the waveguide antenna elements set equal to $\varepsilon_r = 10.23$.

using the actual lengths for the pins (L_5+L_8) and the dielectric cover of the pins ($L_5 - L_{13}$) indicated in Table 6.

The analysis with the new dimensions revealed that the aforementioned manufacturing errors primarily affect the impedance matching characteristics at the input ports (see Fig. 15), whereas the coupling coefficients and radiation patterns remain effectively unchanged.

Fig. 16 shows different views of the manufactured prototype. The physical body of the array demonstrator is

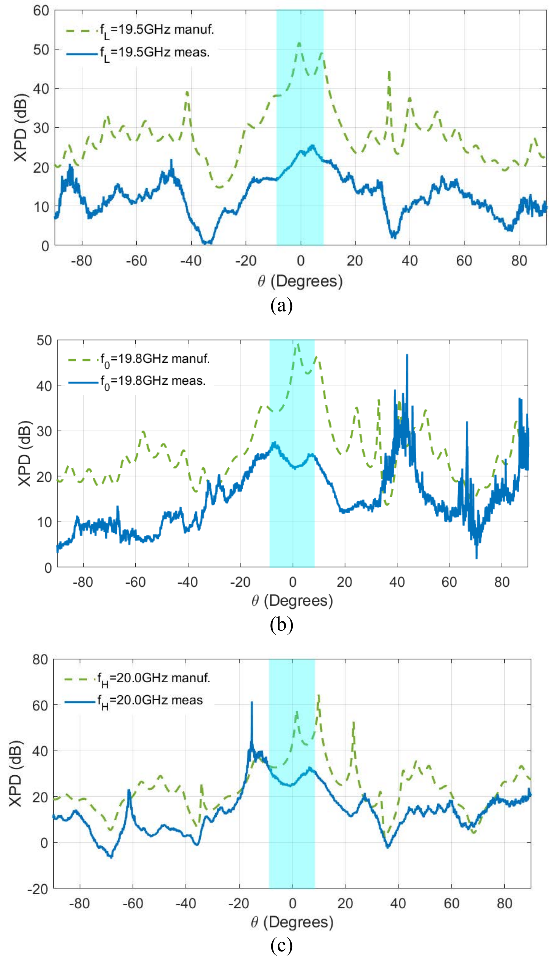

FIGURE 19. Measured (solid line) and simulated (dashed line) XPD of the central sub-array of 3 sub-arrays antenna array at (a) $f_L = 19.5$ GHz, (b) $f_0 = 19.8$ GHz, and (c) $f_H = 20.0$ GHz. The simulation model is based on dielectric parts with relative permittivity $\varepsilon_r = 10.23$.

made of aluminum and machined through a computer numerical control (CNC) milling process. The feeding structures have been manufactured separately and then mounted on the main structure with screws. The supporting pillars have been realized out of aluminum as well, whereas the base plate is made out of stainless steel. The dielectric rods are milled out of a dielectric sheet with relative permittivity $\varepsilon_r = 10.0$ ($\pm 5\%$).

The experimental measurements revealed a shift in the frequency response of the array demonstrator. The reason for such a shift is likely caused by the tolerance range of $\pm 5\%$ in the permittivity of the dielectric material used for the fabrication. By numerical fitting, we concluded that the actual relative permittivity is around $\varepsilon_r = 10.23$.

The measured scattering parameters of the array demonstrator are shown in Fig. 17 and compared to those of the updated simulation model with the fitted relative dielectric constant. A residual deviation between measured and simulated S_{11}, S_{22}, and S_{33} parameters can be observed. This is due to manufacturing inaccuracies which resulted in air gaps in the feeding structure. On the other hand, the reported in Fig. 18 measured and simulated radiation patterns successfully demonstrate the achievement of flat-top characteristics over almost the entire frequency band of operation.

The measured XPD is shown in Fig. 19 and it is compared to the equivalent figure of merit relevant to the complete array inclusive of feeding and holding structures as shown in Fig. 14 while accounting for the deviations between the simulated model and the manufactured prototype. As can be seen in Fig. 19, the inclusion of the feeding and the holding structures results in a reduced XPD level of about 30dB, in the worst-case scenario, across the main-beam region. The measured XPD results tend to match the simulated XPD behavioral trend, but are typically lower, although above 20dB across nearly the entire main-beam region with a small additional degradation at 19.5 GHz.

V. CONCLUSION

A reactively loaded antenna array with enhanced bandwidth characteristics was presented. The proposed design relies on dielectric-based radiating elements which support enhanced inter-element coupling which, in turn, translates into better control of the sub-array characteristics. The manufactured sub-array structure features a fairly stable flat-top radiation pattern over an operational bandwidth of about 500 MHz, from 19.7 GHz to 20.2 GHz. Relevant analyses revealed a strong overlapping effect, occurring between sub-arrays, which is instrumental to enhance the array directivity. A three-element array based on the designed sub-array was manufactured and characterized.

The flat-top radiation pattern behavior with low sidelobe levels across the operating frequency band has been successfully demonstrated. The measurements showed the importance of accurate manufacturing of the feeding structure to reduce performance deviations, especially in terms of input impedance matching characteristics.

REFERENCES

[1] W. Hong, Z. H. Jiang, C. Yu, J. Zhou, P. Chen, Z. Yu, H. Zhang, B. Yang, X. Pang, M. Jiang, and Y. Cheng, "Multibeam antenna technologies for 5G wireless communications," *IEEE Trans. Antennas Propag.*, vol. 65, no. 12, pp. 6231–6249, Dec. 2017, doi: 10.1109/TAP.2017.2712819.

[2] G. Federico, D. Caratelli, G. Theis, and A. B. Smolders, "A review of antenna array technologies for point-to-point and point-to-multipoint wireless communications at millimeter-wave frequencies," *Int. J. Antennas Propag.*, vol. 2021, pp. 1–18, Apr. 2021.

[3] J. S. Herd and M. D. Conway, "The evolution to modern phased array architectures," *Proc. IEEE*, vol. 104, no. 3, pp. 519–529, Mar. 2016, doi: 10.1109/JPROC.2015.2494879.

[4] P. Angeletti and M. Lisi, "Multimode beamforming networks for space applications," *IEEE Antennas Propag. Mag.*, vol. 56, no. 1, pp. 62–78, Feb. 2014, doi: 10.1109/MAP.2014.6821760.

[5] D. Petrolati, P. Angeletti, and G. Toso, "A lossless beam-forming network for linear arrays based on overlapped sub-arrays," *IEEE Trans. Antennas Propag.*, vol. 62, no. 4, pp. 1769–1778, Apr. 2014, doi: 10.1109/TAP.2013.2282189.

[6] P. Angeletti, G. Toso, and D. Petrolati, "Beam-forming network for an array antenna and array antenna comprising the same," U.S. Patent 9 374 145, Nov. 26, 2012.

[7] H. E. A. Laue and W. P. Du Plessis, "A checkered network for implementing arbitrary overlapped feed networks," *IEEE Trans. Microw. Theory Techn.*, vol. 67, no. 11, pp. 4632–4640, Nov. 2019, doi: 10.1109/TMTT.2019.2940223.

[8] R. Harrington, "Reactively controlled directive arrays," *IEEE Trans. Antennas Propag.*, vol. AP-26, no. 3, pp. 390–395, May 1978, doi: 10.1109/TAP.1978.1141852.

[9] Y. Chen and C.-F. Wang, "Reactively loaded antenna array design with characteristic modes and DE algorithm," in *Proc. IEEE Int. Symp. Antennas Propag.*, Jul. 2012, pp. 1–2, doi: 10.1109/APS.2012.6348999.

[10] J. Luzwick and R. F. Harrington, "A reactively loaded aperture antenna array," *IEEE Trans. Antennas Propag.*, vol. AP-26, no. 4, pp. 543–547, Jul. 1978, doi: 10.1109/TAP.1978.1141880.

[11] F. Arndt, K.-H. Wolff, L. Brunjes, R. Heyen, F. Siefken-Herrlich, W. Bothmer, and E. Forgber, "Generalized moment method analysis of planar reactively loaded rectangular waveguide arrays," *IEEE Trans. Antennas Propag.*, vol. 37, no. 3, pp. 329–338, Mar. 1989, doi: 10.1109/8.18729.

[12] S. P. Skobelev, *Phased Array Antennas With Optimized Element Patterns*. Norwood, MA, USA: Artech House, 2011.

[13] A.-S. Kaddour, J. Milbrandt, C. Menudier, M. Thevenot, P. Pouliguen, P. Potier, and M. Romier, "Performances of magneto-electric dipoles in an antennas array with a reduced beam forming network," in *Proc. 49th Eur. Microw. Conf. (EuMC)*, Oct. 2019, pp. 385–388.

[14] N. T. Nguyen, R. Sauleau, and L. Le Coq, "Reduced-size double-shell lens antenna with flat-top radiation pattern for indoor communications at millimeter waves," *IEEE Trans. Antennas Propag.*, vol. 59, no. 6, pp. 2424–2429, Jun. 2011, doi: 10.1109/TAP.2011.2144554.

[15] R. Eirey-Perez, A. A. Salas-Sanchez, J. A. Rodriguez-Gonzalez, E. Moreno-Piquero, and F. J. Ares-Pena, "Pencil beams and flat-topped beams with asymmetric side lobes from circular arrays," in *Proc. 8th Eur. Conf. Antennas Propag. (EuCAP)*, Apr. 2014, pp. 3615–3619, doi: 10.1109/EuCAP.2014.6902612.

[16] H. Wang, Z. Zhang, Y. Li, and M. Iskander, "A switched beam antenna with shaped radiation pattern and interleaving array architecture," *IEEE Trans. Antennas Propag.*, vol. 63, no. 7, pp. 2914–2921, Jul. 2015, doi: 10.1109/TAP.2015.2422838.

[17] Z.-Y. Zhang, N.-W. Liu, S. Zuo, Y. Li, and G. Fu, "Wideband circularly polarised array antenna with flat-top beam pattern," *Microw., Antennas Propag.*, vol. 9, no. 8, pp. 755–761, Jun. 2015, doi: 10.1049/iet-map.2014.0689.

[18] U. A. Pawar, S. Chakraborty, T. Sarkar, A. Ghosh, L. L. K. Singh, and S. Chattopadhyay, "Quasi-planar composite microstrip antenna: Symmetrical flat-top radiation with high gain and low cross polarization," *IEEE Access*, vol. 7, pp. 68917–68929, 2019, doi: 10.1109/ACCESS.2019.2918580.

[19] H.-T. Chou, Y.-S. Chang, H.-J. Huang, Z.-D. Yan, T. Lertwiriyaprapa, and D. Torrungrueng, "Two-dimensional multi-ring dielectric lens antenna to radiate fan-shaped multi-beams with optimum adjacent-beam overlapping crossover by genetic algorithm," *IEEE Access*, vol. 8, pp. 79124–79133, 2020, doi: 10.1109/ACCESS.2020.2990223.

[20] R. T. Maximidis, D. Caratelli, G. Toso, and A. B. Smolders, "Design of overlapped subarrays based on aperture reactive loading," *IEEE Trans. Antennas Propag.*, vol. 68, no. 7, pp. 5322–5333, Jul. 2020, doi: 10.1109/TAP.2020.2981739.

[21] S. Steshenko, M. Zhadobov, R. Sauleau, A. A. Kirilenko, and A. V. Boriskin, "Beam-forming capabilities of waveguide feeds assisted by corrugated flanges," *IEEE Trans. Antennas Propag.*, vol. 63, no. 12, pp. 5548–5560, Dec. 2015, doi: 10.1109/TAP.2015.2487990.

[22] R. T. Maximidis, A. B. Smolders, G. Toso, and D. Caratelli, "Planar reactively loaded array antenna with flat-top radiation pattern characteristics," in *Proc. IEEE Int. Symp. Antennas Propag. North Amer. Radio Sci. Meeting*, Jul. 2020, pp. 2091–2092, doi: 10.1109/IEEECONF35879.2020.9330061.

[23] Mathworks. (2017). MATLAB. [Online]. Available: www.MATLAB.com

[24] R. Maximidis, D. Caratelli, G. Toso, and A. B. Smolders, "High-gain planar array of reactively loaded antennas for limited scan range applications," *Electronics*, vol. 9, no. 9, p. 1376, Aug. 2020, doi: 10.3390/electronics9091376.

[25] R. J. Mailloux, *Phased Array Antenna Handbook*. Norwood, MA, USA: Artech House, 2005.

[26] Dassault Systems. (2019). *CST 2019*. [Online]. Available: https://www.cst.com/

RONIS MAXIMIDIS was born in Tbilisi, Georgia, in 1984. He received the Diploma degree (Hons.) in electrical and computer engineering and the master's degree (Hons.) in communication and satellite telecommunication systems from the Democritus University of Thrace, Xanthi, Greece, in 2011 and 2014, respectively, and the Ph.D. degree from the Eindhoven University of Technology, in 2021. From 2010 to 2014, he worked on the development of a technique for characteristic mode analysis of the composite metal-dielectric structure and its use for MIMO antenna design. His Ph.D. work on the development of the design techniques of multibeam antenna arrays with significantly reduced mass volume and cost. The work was performed in the framework of the project "Multibeam Antenna with Overlapped Subarray" and was supported by European Space Agency (ESA) and The Antenna Company. Since 2021, he has been working as a Researcher at the Aristotle University of Technology, Greece. His research focus is on the convergence of fiber-wireless networks and on free-space optical communication. His research interests include electromagnetics, wireless transmission, antennas, and antenna arrays, including optical antennas and photonic and photonic assisted beamformers.

DIEGO CARATELLI (Senior Member, IEEE) was born in Latina, Italy, in 1975. He received the Laurea *(summa cum laude)* and Ph.D. degrees in electronic engineering and the M.Sc. degree *(summa cum laude)* in applied mathematics from the Sapienza University of Rome, Rome, Italy, in 2000, 2004, and 2013, respectively.

From 2005 to 2007, he was a Research Fellow with the Department of Electronic Engineering, Sapienza University of Rome. From 2007 to 2013, he was a Senior Researcher with the International Research Center for Telecommunications and Radar, Delft University of Technology, Delft, The Netherlands. From 2015 to 2019, he was an Associate Professor with the Institute of Cybernetics, Tomsk Polytechnic University, Tomsk, Russia. In 2013, he co-founded The Antenna Company, Eindhoven, The Netherlands, where he is currently the Chief Technology Officer/the Vice-President of Engineering and is responsible for product development, program portfolio management, and technical direction of the engineering team. Since 2020, he has been an Associate Professor with the Group of Electromagnetics in Wireless Telecommunications, Eindhoven University of Technology, Eindhoven. He has authored or coauthored more than 200 publications in international peer-reviewed journals, book chapters, and conference proceedings. He holds 22 families of patents in antenna-related technologies and advanced computational techniques. His current research interests include the full-wave analysis and design of passive devices and antennas for satellite, wireless, and radar applications, the development of analytically-based numerical techniques devoted to the modeling of wave propagation and diffraction processes, the theory of special functions for electromagnetics, the deterministic synthesis of sparse antenna arrays, and the solution of boundary-value problems for partial differential equations of mathematical physics.

Dr. Caratelli is currently a member of the Applied Computational Electromagnetics Society (ACES), the Institution of Engineering and Technology (IET), the International Union of Radio Science (URSI), the Italian Electromagnetic Society (SIEm), and the Institute of Electrical and Electronics Engineers (IEEE). He was a recipient of the Young Antenna Engineer Prize at the 32nd European Space Agency Antenna Workshop and the 2010 Best Paper Award from ACES. He was a co-recipient of the Frost and Sullivan Best Practices Award for technology innovation in advanced antennas for wireless communications in 2016. He is the Lead Guest Editor of the Special Issue on Advanced Antenna Array Development for mm-Wave Communications of *International Journal of Antennas and Propagation* (Hindawi), and the Special Issue on Theory and Applications of Special Functions in Mathematical Physics of *Symmetry* (MDPI).

GIOVANNI TOSO (Senior Member, IEEE) received the Laurea *(cum laude)* and Ph.D. degrees from the University of Florence, Italy, in 1992 and 1995, respectively. He received the Postdoctoral Fellowship from the University of Florence, in 1999. He spent more than one year as a Visiting Scientist at the Laboratoire d'Optique Electromagnétique, Marseille, France. In 1999, he was a Visiting Scientist at the University of California (UCLA) at Los Angeles. He received a scholarship from Alenia Spazio, Rome, Italy, and he has been appointed as a Researcher in a radio astronomy observatory of the Italian National Council of Researches (CNR). Since 2000, he has been with the Antenna and Submillimeter Waves Section, European Space Agency, ESA ESTEC, Noordwijk, The Netherlands. He has been initiating several research and development activities on satellite antennas based on arrays, reflectarrays, discrete lenses, and reflectors. In particular, in the field of onboard satellite antennas, he has been coordinating activities on multibeam antennas, active and passive, mainly at Telecom applications. In the field of terminal antennas for Telecom applications, he has been supporting the development of reconfigurable antennas with electronic, mechanical, and hybrid scanning. Some of these antennas, developed by Viasat, Airbus Italy, Satixfy UK, and Swissto12 are currently available as products. He has promoted the development of the commercial software tool QUPES by TICRA, also used worldwide, for the analysis and design of periodic and quasi-periodic surfaces, such as reflectarrays, frequency selective surfaces, transmitarrays, and polarizers. In 2014, he was a Guest Editor, together with Dr. R. Mailloux, of the Special Issue on innovative phased array antennas based on non-regular lattices and overlapped subarrays published in the IEEE TRANSACTIONS ON ANTENNAS AND PROPAGATION and, for the same society, and an Associate Editor (2013–2016). Since 2006, he has been supporting the European School of Antennas (ESoA) course on Satellite Antennas and indicated as the Best Teacher in the first seven editions of the course. Since 2010, together with Dr. P. Angeletti, he has been instructing short courses on Multibeam Antennas and Beamforming Networks during international conferences (IEEE APS, IEEE IMS, IEEE IWCS, EUCAP, and EuMW) that have been attended by more than 1000 participants. In 2018, he has been the Chairperson of the 39th ESA Antenna Workshop on "Multibeam and Reconfigurable Antennas." In the same year, he received, together with Prof. A. Skrivervik, the 2018 ESoA Best Teacher Award. He is the Organizer of the new ESoA course on Active Antennas. He has been selected as a Distinguished Lecturer for the IEEE Antennas and Propagation Society (2022–2024).

A. BART SMOLDERS (Senior Member, IEEE) was born in Hilvarenbeek, The Netherlands, in 1965. He received the M.Sc. and Ph.D. degrees in electrical engineering from the Eindhoven University of Technology (TU/e), in 1989 and 1994, respectively. From 1989 to 1991, he worked as an IC Designer at FEL-TNO, The Hague. From 1994 to 1997, he was a Radar System Designer with Thales, The Netherlands. From 1997 to 2000, he was the Project Leader of the Square Kilometer Array (SKA) with the Netherlands Foundation for Research in Astronomy (ASTRON). From 2000 to 2010, he was with NXP (formerly Philips) Semiconductors, The Netherlands, responsible for the innovation in the RF business line. Since 2010, he has been a full-time Professor at the Electromagnetics Group, TU/e, with special interest in antenna systems and applications. He currently leads several research projects in the area of integrated antenna systems operating at frequencies up to 150 GHz for several application domains, including 5G/6G wireless communications, radar sensors, and radio-astronomy. He is the Junior-Past Chairman of the IEEE Benelux Section and the Past-Chair of the Nederlands Radio en Elektronica Genootschap (NERG). He is a Board Member of the Stichting Wetenschappelijke Activiteiten van het Nederlands URSI Committee (SWAN) and a member of the Advisory Board of ASTRON and PhotonDelta. Next to his research activities, he is the Dean of the Electrical Engineering Department, TU/e. He has published more than 150 papers. For more information visit the link: (https://www.tue.nl/en/research/researchers/bart-smolders/).